Green and facile recycling of bauxite residue to biochar-supported iron-based composite material for hydrothermal liquefaction of municipal solid waste

Sharma, Kamaldeep; Sadetmahaleh, Komeil Kohansal; Jaime Azuara, Antonio; Rosendahl, Lasse; Benedetti, Vittoria; Yu, Donghong; Pedersen, Thomas Helmer

Published in:
Waste Management

DOI (link to publication from Publisher):
10.1016/j.wasman.2023.08.024

Publication date:
2023

Document Version
Publisher's PDF, also known as Version of record

Waste Management 171 (2023) 259–270

Contents lists available at ScienceDirect

Waste Management

journal homepage: www.elsevier.com/locate/wasman

Research Paper

Green and facile recycling of bauxite residue to biochar-supported iron-based composite material for hydrothermal liquefaction of municipal solid waste

Kamaldeep Sharma [a], Komeil Kohansal [a], Antonio Jaime Azuara [a], Lasse Aistrup Rosendahl [a], Vittoria Benedetti [b], Donghong Yu [c], Thomas Helmer Pedersen [a,*]

[a] Department of Energy, Aalborg University, Pontoppidanstræde 111, 9220 Aalborg Øst, Denmark
[b] Faculty of Science and Technology, Free University of Bolzano, 39100 Bozen-Bolzano, Italy
[c] Department of Chemistry and Bioscience, Aalborg University, Pontoppidanstræde 111, 9220 Aalborg Øst, Denmark

ARTICLE INFO

Keywords:
Bauxite residue
Municipal solid waste
Green reduction
Heterogeneous catalyst
Hydrothermal liquefaction
Biofuels

ABSTRACT

Industrial and municipal wastes remain significant sources of air, soil, and water pollution, thus causing adverse climate and health impacts. EU faces challenges in developing green recycling processes and reducing GHG emissions. Innovation in green catalysis is a key driver toward the fulfilment of these goals. This study demonstrated a single-step "Green Recycling" route by which different wastes e.g., industrial and bioorganic wastes are treated to produce biochar/Fe(0) (BC-Fe(0)) material. Typically, three different biomass namely organic fraction of municipal solid waste (biopulp), wheat straw (WS), and microalgae (MA) were used as green reducing agents for reducing bauxite residue (BR). Among all biomass, the high reduction potential of amino acids present in biopulp facilitated the synthesis of BC-Fe(0). BC-Fe(0) material acted as an effective catalyst for HTL of biopulp as the results showed the highest bio-crude yield (44 wt%) at 300 °C for 30 min with 10 wt% BC-Fe(0) loading (containing 2.5 wt% Fe). Furthermore, BC-Fe(0) also assisted in-situ hydrogenation and deoxygenation of chemical compounds present in the bio-liquid product, therefore bio-crude exhibited a higher H/C ratio (1.73) and lower oxygen contents (9.78 wt%) in comparison to bio-crude obtained without catalyst. However, Raw BR and reduced BR (RED) as catalysts showed no significant effect on the yield and oxygen content of bio-crude, which confirms the high catalytic activity of Fe(0) containing BC-Fe(0). Therefore, this study demonstrates the greener path for the one-step valorization of industrial and organic wastes, as an alternative to existing chemical and high temperature-based waste recycling and catalyst synthesis technologies.

1. Introduction

Hydrothermal liquefaction (HTL) has been introduced as an environmental-friendly technology as it uses water as a reaction medium as well as a catalyst to facilitate biomass conversion. High operation flexibility, energy efficiency, as well as low carbon and sulfur footprints make HTL an environment favourable technology to produce drop-in biofuels (Chen et al., 2018). As estimated by Energy Information Administration (EIA), global energy usage will continue to increase by 50 % by 2050 (International Energy Outlook 2021 Narrative). To meet emerging fuel demand, HTL requires sustainable and reliable biomass resources.

In comparison to first and third-generation biomass, second-generation biomass feedstocks are not in competition with food and do not contribute to substantial investment in resource production (Gasparatos et al., 2013). Sewage sludge and municipal solid waste (MSW) have been considered as key biomass to produce second-generation biofuels due to their ever-increasing abundance and urgent disposal demand. Based on Chen et al. (2020) estimations, the annual MSW generation has persistently increased from 635 Mt in 1965 to 1999 Mt in 2015, and this number will likely rise to 3539 Mt by 2100. Sharma et al. (2020) revealed that depending on geometrical and economic indices, the organic fraction that can be a carbon source for biofuel production accounts for 28 to 58 % of the MSW (Sharma and Jain, 2020). MSW contains non-biodegradable constituents like plastics, glass, and metal, which inhibit its thermochemical processing to

* Corresponding author.
E-mail address: thp@energy.aau.dk (T.H. Pedersen).

https://doi.org/10.1016/j.wasman.2023.08.024
Received 10 January 2023; Received in revised form 20 July 2023; Accepted 23 August 2023
Available online 6 September 2023

biofuels. As a mechanical pretreatment technology, 'Ecogi' process segregates non-biodegradable materials and yields a uniform wet biomass so-called biopulp (Kohansal et al., 2021).

In previous HTL studies, different homogeneous catalysts like inorganic acids and alkali salts have been used to increase biomass conversion efficiency, bio-crude yield, and quality (Posmanik et al., 2018; Ross et al., 2010). Homogeneous alkali catalysts promote the oxygen removal through decarboxylation (—CO_2) and decarbonylation (—CO) pathways, whereas the removal of nitrogen still represents a relevant challenge to be addressed. Despite the former improvements, the utilization of these catalysts in HTL has not proven to be economically and environmentally viable because they must be neutralized before discharge and cannot be easily recovered (Kohansal et al., 2021). These generate additional processing costs and waste resulting from loss of carbon and other by-products in the aqueous phase. Comparatively, heterogeneous catalysts have been widely used for the thermochemical conversion of different biomass due to their unique advantages like high catalytic activity, selectivity, recyclability, and reusability (Scarsella et al., 2020). However, the current industrial heterogeneous catalysts incorporate materials, like platinum metals and rare-earth elements, which are deemed critical by the EU (European Commission, 2020). The synthesis of cheap heterogeneous catalysts from industrial wastes for the improved bio-crude yield and quality is one of the recent developments in bio-fuel production that could make the overall process more efficient and economic. Additionally, heterogeneous catalysts minimize the formation of by-products during the biomass conversion process.

Bauxite residue (BR), which is a landfilled industrial residue from aluminium industry, is experiencing a growth rate of 120 Mt/year globally. If not handled responsibly, it represents an environmental threat for fertile soil and groundwater due to its high alkalinity and caustic contents (Ujaczki et al., 2018). However, BR can provide significant amounts of important transition metals, which can be used to generate catalysts for the catalysis-driven HTL process more cost-effective and environment-friendly in terms of waste-to-energy conversion (Klauber et al., 2009). BR rich in Fe_2O_3, Al_2O_3, CaO, and SiO_2 were already tested in catalytic HTL and pyrolysis of different biomass, obtaining high yield and energy recovery (ER) in bio-crude (Agblevor et al., 2020; Cheng et al., 2020). However, the decrease of heteroatoms in bio-crude was not satisfactory. By developing low-cost, innovative, and sustainable technologies for the recovery of catalytically active metals from BR for the valorization of biomass, cost-competitive biofuels could be obtained.

Previously, the reduction of BR was performed using chemicals, high temperatures (1500–1600 °C), smelting-reduction, and multi-step reduction processes (Cardenia et al., 2019; Wang et al., 2020). Furthermore, the direct functionalization of BR on carbon support was also carried out using HNO_3 acid and multi-step pyrolysis processes to use the resulting composite material as a catalyst (Guo et al., 2021; Yoon et al., 2019). Furthermore, wood, algae and straw biochar have also been used as support for iron zero (Fe(0)) based adsorbers (Zhang et al., 2020; Wang et al. 2023; Wang et al. 2019). These synthesis methods are not convenient to cope with climate challenges of industrial wastes and catalysts production on large-scale industrial processes. Therefore, the development of facile and innovative approaches is required for the synthesis of green catalysts to achieve a sustainable and circular economy.

In the present study, a single-step "Green Recycling" method is developed for the direct recovery of Fe(0) from BR without using any additive. Typically, as received BR is mixed with dry biopulp, and the resulting mixture is heated in a solid-state under a nitrogen atmosphere to obtain biochar-supported Fe(0) (BC-Fe(0)) material. By moving one step forward, the BC-Fe(0) composite material was utilized as a catalyst for the HTL of biopulp. BC-Fe(0) material was tested for in-situ hydrogenation of heteroatoms containing compounds in biopulp aiming: 1) to enhance bio-crude yield through minimizing carbon loss occurs through —CO and —CO_2 pathways and 2) improving bio-crude properties by facilitating catalytic transfer hydrogenation reaction. The role of Fe(0) in the removal of heteroatoms through hydrogenation and improving the quality and yield of bio-crude was verified by using raw BR and reduced BR as catalysts under the same conditions. Hence, this manuscript explores a new greener path for the recovery of catalytically active iron metal from hazardous industrial waste for biomass valorization, as an alternative to current chemical and high temperature-based catalyst synthesis processes from industrial wastes.

2. Material and methods

2.1. Bauxite residue and biomass feedstocks

The BR used in this study was obtained from Mytilineos Holdings S. A, Greece, which contains Fe_2O_3 (~50 %), Al_2O_3 (11–25 %), SiO_2 (4–15 %), TiO_2 (4–8 %), Na_2O (1.5–5 %) and CaO (4–15 %). Different biomass like biopulp (BP), wheat straw (WS), and Seaweed L. digitate macroalgae (MA) were investigated for the synthesis of BC-Fe(0) material. These feedstocks were obtained from the Ecogi process (Kohansal et al., 2021), wheat crop field located in Denmark (Seehar et al., 2020), and the Ocean Rainforest, Faroe Islands (Sintamarean et al., 2017), respectively. For the catalyst synthesis, MA and WS were dried and ground through a cyclone mill, (Foss, Cyclotec 1093, Hillerød, Denmark) and screened with the help of the sieves in the range between 0.5 and 1.0 mm size. In contrast, BP was dried and used directly without any further processing as it has already gone through a mechanical pretreatment at Gemidan A/S, Denmark (Kohansal et al., 2021a). Detailed analyses of all three biomass were carried out to determine the elemental composition and quantitative properties of biomass (Table S1). XRD spectrum of BR was also recorded to perform the mineralogical analysis.

2.2. Catalyst synthesis procedure

Prior to use in the synthesis process, BR was dried at 105 °C overnight. Three biomass feedstocks with diverse chemical compositions namely BP, WS, and MA were used as reducing agents for the single-step reduction of BR to Fe(0). Six different dry homogeneous mixtures containing BR and each feedstock (i.e., BP, WS, and MA) in two different proportions (1:1 and 1:2 m/m) were prepared by simple mixing. The mixtures were then heated at a rate of 5 °C min^{-1} in a quenching furnace under an N_2 atmosphere until the required temperature of 700 °C was reached and maintained for 5 h. The obtained powdered mixtures were characterized using XRD, SEM, elemental mapping, and TGA to confirm the reduction of BR to Fe(0). After the characterization, BC-Fe(0) obtained from BR-BP (1:2) was only used as catalyst for catalytic HTL of BP because materials obtained from BR-WS and BR-MA mixtures did not show presence of Fe(0). To compare the catalytic activity of BC-Fe(0) material, reduced bauxite residue (RED) was also synthesized by reducing BR in a micro-batch reactor at 400 °C under 8 MPa H_2 pressure for 30 min. RED was used as a catalyst in HTL experiments. For the catalytic HTL experiment, 10 wt% or 20 wt% overall loading (including fixed carbon if present) of BC-Fe(0), BR and RED was used, which were denoted as Fe(0)-10 %, Fe(0)-20 %, BR-10 %, and RED-10 %, respectively, as shown in Fig. 5.

2.3. Catalyst characterization

Morphological and elemental mapping analyses of BR and composite material were performed using SEM (Zeiss EVO 60). XRD patterns of powder samples were studied using a PANalytical empyrean X-ray diffractometer equipped with CuKα targets at a scanning rate of $2\theta = 2^{\circ}$ min^{-1}, the wavelength of 0.154 nm, a voltage of 40 kV and a step size of 0.013°. FTIR spectra of materials were recorded to determine the functional groups in the biomass and their interactions with BR by using a Bruker TENSOR II spectrometer, in the range of 4000 to 400 cm^{-1}. Thermal stability and thermal degradation of all the catalytic material

were measured by performing TGA up to 1000 °C using TA Instruments Discovery, Netzsch STA 409 PC, Netzsch STA 409 PC. All the samples were analysed under oxygen atmospheres between 30 and 1000 °C at a heating rate of 10 °C/min. Carbon content in BC-Fe(0) composite material was measured using PerkinElmer CHN–O analyzer model 2400 Series II. Specific surface area, pore volume, and pore size of samples were measured using a 3Flex Surface Characterization Analyzer (Micromeritics Co.) operating with N_2 at −196 °C. Before analysis, samples were firstly degassed ex situ with N_2 at ambient temperature for three hours and then at 125 °C overnight. Subsequently, samples were vacuum degassed in situ at 125 °C for four hours. The specific surface area was determined by the Brunauer-Emmett-Teller (BET) method (Brunauer et al., 1938), while the total pore volume and the average pore size were obtained by the Barret-Joyner-Halenda (BJH) desorption analysis (Barrett et al., 1951).

2.4. Catalytic HTL and separation procedures

HTL experiments were performed in 12 ml micro-batch reactors in duplicates. The reactor was initially charged with 7 g of biopulp (1.09 g of dry matter). In a typical catalytic run, the specific amount of each catalyst (10 wt% or 20 wt% dented as 10 % and 20 %, respectively) was additionally loaded into the reactor. Before dipping the reactors into the fluidized sand bath (Techne, SBL-2D), reactors were purged with nitrogen gas and pressurized to 1.5–2.0 MPa. The bottom part of the reactor was then inserted in the sand bath heated at the desired reaction temperature, while the top part was connected to a mechanical agitator, providing the necessary mixing throughout the desired reaction time. After maintaining at the specified temperature (300 °C) for 30 min (residence time), the reactors were promptly quenched in the water bath to force sudden termination of hydrothermal reactions. To ensure the reproducibility of the obtained results, each HTL experiment with the same sample was performed under the same conditions in duplicates by using two identical reactors.

The separation method is comprehensively elaborated in previous studies (Kohansal et al., 2021a). Briefly, HTL product separation was initiated by monitoring the produced pressure and subsequently gas collected for GC analysis. Afterward, the reactor was opened, and the aqueous phase together with some solids was filtered through a filter paper (5–13 μm), and the filtered aqueous phase was stored for further analyses. The sticky bio-crude phase was rinsed with 25–40 ml of DCM. The mixture was filtered through the previously used filter paper, and the collected solid phase was oven-dried at 105 °C overnight. It means that volatile compounds should either be soluble in the DCM solvent ending up in bio-crude or be evaporated when drying the solid residue. Thus, it is a reasonable assumption that the solid residue consists only fixed carbon and inorganics. Thereafter, the DCM-bio-crude mixture was evaporated through vacuum evaporation (Büchi R210) and the weight of produced bio-crude was determined. In this article, the HTL products' yield are described on dry ash-free (daf) basis as per the equations given below.

$$\text{Biocrude yield}_{daf}\,(\%) = (\text{Weight of biocrude}_{daf}\,/\text{Weight of biomass used}_{daf}) \times 100 \quad (1)$$

$$\text{Solid yield}_{daf}\,(\%) = (\text{Weight of solid recovered}_{daf} - \text{Weight of carbon in catalyst}_{daf})\,/\text{Weight of biomass used}_{daf}) \times 100 \quad (2)$$

$$\text{Gas yield}\,(\%) = (\text{Weight of gases}/\text{Weight of the biomass used}_{daf}) \times 100 \quad (3)$$

$$\text{HHV}\ (\text{MJ/kg}) = (0.335)\text{C} + (1.423)\text{H} - (0.154)\text{O} - (0.145)\text{N} \quad (4)$$

$$\text{Energy Recovery, ER}\,(\%) = (\text{HHV of product}/\text{HHV of biomass used}) \times \text{biocrude yield} \quad (5)$$

For the calculation of gas yield, the weight of the gases produced was calculated by weighing the reactor before and after the HTL process. The solid yield is calculated as dry ash free basis, and the carbon from the catalyst is also removed from the weight of recovered solids during HTL process as presented in Equation (2).

2.5. Characterization of HTL products

The elemental composition of bio-crudes and solid residues was measured using PerkinElmer analyzer (USA-2400 Series II CHN) in conformity with ASTM D5291. The oxygen content was computed by difference. HHV and ER were calculated based on equations reported elsewhere (Taghipour et al., 2021). GC–MS (Thermo Scientific, Trace 1300, and ISQ-ID, respectively) equipped with a CP-9036 capillary column (5 % phenyl 95 % dimethylpolysiloxane, 20 m × 0.15 mm × 0.15 lm) was employed to characterize volatile fraction (<300 °C) of bio-crude following the procedure reported by Conti et al., (2020). The percentage peak area method was used to determine the approximate concentration of each compound belonging to different functional groups. Furthermore, functionalities in bio-crudes were explored via FT-IR (Bruker TENSOR II) instrument. A TGA system (Discovery SDT 650) analysis instrument was used to detect the boiling point distribution, volatile matter, and ash contents of solid residues and bio-crudes under a nitrogen atmosphere followed by an oxygen environment between 30 and 775 °C at a heating rate of 10 °C/min. ^{13}C NMR spectra were recorded on a BRUKER AVIII-600 MHz NMR spectrometer equipped with a cryogenically cooled, triple-resonance CPP-TCI probe. The ^{13}C nuclei were ^{1}H-decoupled using the Waltz-16 composite pulse decoupling scheme. Carbon spectra were acquired at 150.78 MHz with 30°-pulses, a spectral width of 36 kHz, collecting 16,000 scans using relaxation delay of 4.0 sec resulted in a good signal-to-noise ratio after 10 h of total time of measurement per sample. Total organic carbon (TOC) and total nitrogen (TN) of aqueous phase by-products was measured through LCK386 HACH kits assisted by a spectrophotometer (HACH & Lange, DE3900). Additionally, employing a pH meter (WTW 3210), the basicity of water phase samples was measured. The composition of the gaseous products was studied using a GC-2010 gas chromatograph (Shimadzu Inc.) equipped with a GC-BID detector.

3. Results and discussion

3.1. Synthesis and characterization of BC-Fe(0) composite material

3.1.1. Effects of feedstocks on the reduction of BR

Three sustainable feedstocks with different chemical compositions were selected and used as reducing agents for the reduction of BR. These feedstocks are rich in lignocellulosic (WS), lipids, and proteins (BP and MA). Among all the three feedstocks, BP contains a higher concentration of easily degradable organics like protein and lipid, while lignocellulose is the main organic component of WS (Table S1). Lignocellulosics are difficult to degrade owing to the complex structure of their components like lignin, cellulose, and hemicellulose (Wang et al., 2018). Amino acids present in the protein as a main component of BP, contain electron-donating amino groups (—NH_2 group), which preferentially can coordinate with the central Fe(III)/Fe(II) ion and facilitate its reduction to Fe (0) (Klačanová et al., 2013). Furthermore, the high pH of BR deprotonates the carboxylic acid groups in amino acids and induces the formation of electron donor carboxylate anion O═C—O^-, which further facilitates the reduction of BR (Afonso et al., 1990). On the other hand, lipid head groups containing polar molecules interact directly with the metal ions, which may lead to the enhanced chemical reactivity of the

metal ions for the reduction process (Ansari et al., 2021; Wang and Liu, 2014). Fig. 1A shows the XRD spectra of BR and BR treated with all three feedstocks in different proportions. The XRD spectra of BR treated with BP (BR-BP (1:2)) showed the disappearance of characteristic peaks of hematite (Fe_2O_3) at 33.6° and 35.5° and the appearance of typical peaks of Fe(0) at around 44.6 and 65.1° 2θ angles, which confirmed the existence of Fe(0) as the main component in this BC-Fe(0) composite material synthesized with 1:2 BR:BP mass ratio. These peaks were less intense in the case of BP used in a lower proportion (BR-BP (1:1)). However, these typical peaks with lower intensity were also observed along with the peak corresponding to magnetite (Fe_3O_4) at 35° when MA was used as a reducing agent, which indicated the partial reduction of BR to Fe_3O_4 and Fe(0) in presence of MA. In the case of WS, the XRD spectrum only showed a prominent peak at 35° corresponding to the Fe_3O_4, which indicated that the lignocellulosic induce the incomplete reduction of BR. The results obtained for BP and MA indicate that the proportion of protein and lipid contents in the biomass play an important role in the reduction of BR to Fe(0).

As mentioned in section 2.2, BR was also reduced through the conventional method using H_2 for the comparison of the catalytic activity of the main material. The XRD spectrum of resulting reduced BR (RED) shows the presence of Fe_3O_4, indicating the incomplete reduction of BR in presence of H_2 (Fig. S1).

The FTIR spectra of BR processed with different biomasses are given in Fig. 1B, which were compared with the spectrum of BR as reported in the literature (Wang et al., 2020). The characteristic peaks of BR at 975, 1112, and 3430 cm^{-1} correspond to Si—O, Si—O—Al, and —OH groups, respectively, which were continued in FTIR spectra of BR treated with different biomasses. The stretching vibrations at 580–620 and 705 cm^{-1} correspond to the Al—O—Al and Al—O bonds, respectively in minerals of BR. BR treated with MA and WS shows peaks at 450 and 521 cm^{-1}, which correlate to the Fe—O bond of Fe_2O_3, and Fe_3O_4, indicating the incomplete reduction of BR (Ouyang et al., 2017). However, these peaks are lower in intensity in the case of BR treated with BP, which indicates the severe reduction of BR to Fe(0) in presence of BP. Additionally, the stretching vibration at 1200 cm^{-1}, corresponding to the C—O bond of phenol present in biomass, completely disappeared in the case of BR treated with BP, compared with other feedstocks, which might be due to the removal of polar functional groups during co-precipitation of Fe(0) (Saffari, 2018). The FTIR spectrum of BP was also recorded to compare its transmittance with other BP-containing samples and determine its chemical structure change during the reduction of BR (Fig. 1B). The stretching vibration at 3304 cm^{-1} is owing to the NH or OH groups. Two sharp bands at 2923 and 2853 cm^{-1} are attributed to the symmetric and asymmetric stretching modes of CH_3 and CH_2 groups, respectively. Furthermore, two bands at 1737 and 1646 cm^{-1} are due to the C═O stretching vibrations of ester or carboxylic acid groups and amides, respectively. The main peaks of BP in the FTIR spectrum of BP-BR completely disappeared, which is due to the thermal decomposition of carbon-containing functional groups into CO and CO_2, assisting the reduction of BR. These results show the effectiveness of BP in the reduction of BR to Fe(0) over other biomass feedstocks.

TGA and DTG spectra of all catalytic materials were also recorded under an air atmosphere to analyze their thermal stability and thermal degradation profiles (Fig. 1C and 1D). In the TGA spectrum of BR, the first stage of weight loss up to 100 °C is attributed to the evaporation of water. The second stage of weight loss at around 300 °C accounts for the loss of water of crystallization present within the crystalline structure of minerals in BR. The third and fourth stages of weight loss are due to the thermal decomposition of carbonate minerals (Klačanová et al., 2013). The increase in mass experienced by the synthesized samples at around 300 °C can be attributed to the oxidation of Fe(0) and magnetite (Fe_3O_4) in the presence of air (Masud et al., 2020). This suggests the feedstocks induced a complete and partial reduction of BR. The weight loss after 600 °C in all samples is ascribed to the loss of the fixed carbon present in all the feedstocks. The last stage of weight loss in the case of different

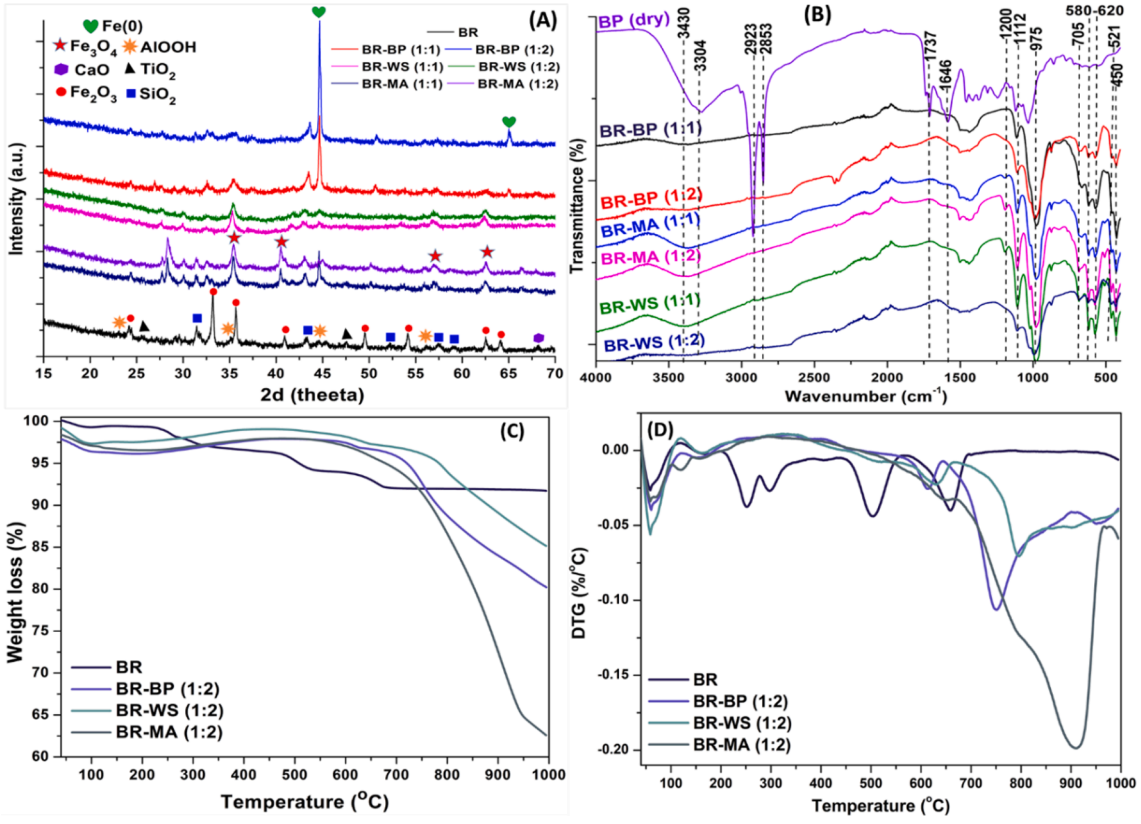

Fig. 1. (A) XRD (B) FTIR (C) TGA and (D) DTG spectra of BR and BR treated with different biomass in a different composition.

biomass and BR mixtures, depending on the fixed carbon contents, is due to the solid decomposition at a temperature range of 600–900 °C, which is caused by the decomposition of carbonaceous matters in the solid residue at a very slow rate. Fig. 1D reports the DTG spectra of BR in presence of different biomass, which show the carbon-thermal reduction temperature of the Fe with biomass. Two distinct peaks in DTG spectrum of BR-BP (1:2) at around 600 °C and 750 °C attributed to the formation of CO_2 and CO, respectively, as shown in the following equations (Mombelli et al., 2019).

$$C + O_2 \rightarrow CO_2 \quad (6)$$

$$2C + O_2 \rightarrow 2CO \quad (7)$$

Furthermore, the produced CO led to the reduction of BR (Fe_2O_3) to Fe in a series of reactions. The first step is a single-step reaction $Fe_2O_3 \rightarrow Fe_3O_4$ and the second part is a combination of two-step reactions: $Fe_3O_4 \rightarrow FeO$ and $FeO \rightarrow Fe$ (Chen et al. 2017).

$$3Fe_2O_3 + CO \rightarrow 2Fe_3O_4 + CO_2 \quad (8)$$

$$Fe_3O_4 + 4CO \rightarrow 3Fe + 4CO_2 \quad (9)$$

The peak attributed to the CO_2 production was also observed in the DTG spectra of BR-WS (1:2) and BR-MA (1:2), however, the peak corresponding to CO was missing in both spectra. This finding confirms the role of BP in the complete reduction of BR.

3.1.2. Mechanistic pathway of reduction of BR to Fe(0)

The detailed composition and elemental analysis of all the feedstocks are presented in supporting information (Table S1). Among three different waste feedstocks used for the reduction of BR, BP contains a higher amount of lipids (19.20 wt%) and proteins (20.60 wt%), which are known to have mild catalytic properties and metal oxide stabilization sites (e.g. –COOH and -RCOOR) (Guo et al., 2021; Limo et al., 2018). These functional groups interact with Fe of the hematite (Fe_2O_3) and their mild catalytic activity facilitates the one-pot reduction of metal oxides at lower temperatures (700 °C) than the ones used in conventional methods.

At high temperatures, the anions of the amino groups ($–NH_2$) in amino acids bind to the Fe(III) in hematite present in BR, and a concerted redox reaction takes place both at the central cation Fe(III) and the associated amino acid ligands bound to the hematite (Fig. 2).

The amino acids are oxidized at the α-carbon atom simultaneously producing formate anions and amides. The resulting produced amides contain one carbon atom shorter than the parent amino acid. Since the reaction occurs simultaneously at both anions of the amino acid bound at the axial sites, the formate anions may reduce Fe(III) to Fe(0) by the single-electron transfer mechanism under the production of CO_2 (Afonso et al., 1990). The proposed mechanism explicates the formation of Fe(0) and amides of carboxylic acids.

The thermal treatment of BR in presence of BP was carried out under both N_2 and O_2 (air) atmospheres in order to elucidate the influence of gaseous atmosphere on iron oxide (Fe_2O_3) reducibility and the probable reduction pathway of BR to Fe(0). The BR treated under air atmosphere did not exhibit the presence of Fe(0) based on the XRD spectrum (Fig. S3). Instead, the characteristic peak of Fe(0) was detected when BR was treated under N_2. This result revealed the re-oxidation of Fe(0) to hematite under O_2 atmosphere due to the reversible oxidation–reduction nature of the metal oxides.

3.1.3. Morphology and structure of BC-Fe(0) composite material

SEM analysis of both BR and BC-Fe(0) composite material was carried out to elucidate their morphologies (Fig. 3A and 3B). SEM image of BR shows the irregular morphology with the small-sized aggregated particles. However, the reduction of BR with BP caused the decrease in particle size as shown in Fig. 3B, which generally results in an increase of active surface area and catalytic activity of the catalytic material. The decrease in particle size of BC-Fe(0) material was also confirmed from the specific surface area by BET analysis (Table S2). The observed morphology of the BC-Fe(0) composite material was found to be nearly spherical, which again indicates the high catalytic activity potential of the catalytic material.

The elemental mapping images (Fig. 3C-F) of the BC-Fe(0) composite evidence that catalytic active Fe metal is finely dispersed on the carbon. However, other elements like calcium, aluminium, silicon, and titanium are also present in traces, which are not shown here. Moreover, a compact distribution of the C, O, and Fe elements at the edges suggesting Fe metal is encapsulated by carbon support, which is favourable for efficient charge carrier separation.

3.1.4. Surface properties of BC-Fe(0) composite material

Physisorption (BET) analysis results are reported in Table S2. The highest value for BET surface area was measured for sample BC-Fe(0) (70 m^2/g), while other samples show low surface areas in the range 14 – 18 m^2/g. As we know that the specific surface area increases with decreasing particle size and the specific surface area is also increased if the particle has pores. The higher specific surface area of BC-Fe(0) material thus indicates its lower particle size. The highest value for total pore volume (0.32 cm^3/g) was registered for BR–WS followed by BR–BP (0.29 cm^3/g). Regarding the average pore size, BR–BP (BC-Fe(0)) is the only sample with pores in the range of mesopores (2 – 50 nm), while other samples show pores in the range of macropores (>50 nm).

The macroporous nature of all samples, except BR–BP, is also confirmed by the shape of the adsorption–desorption isotherms as shown in Fig. 4. Isotherms overlap showing a small hysteresis at p/p0 > 0.4 and taking on a hyperbolic shape at p/p0 > 0.9, due to the presence of macropores. Hysteresis is more evident for BR BP the isotherm of which does not overlap with the ones of other samples, indicating a greater presence of mesopores and a more-developed porous structure of the material. The presence of mesoporosity is confirmed by the peak occurring at around 3 nm except for sample RED. However, curves

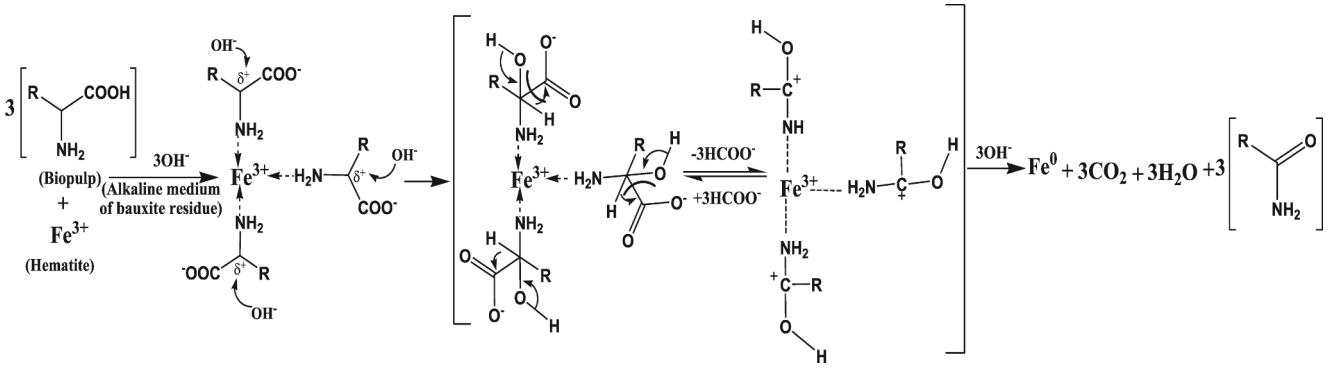

Fig. 2. Suggested mechanism of the reduction of Fe(III) to Fe(0) with amino acid ligands present in biopulp.

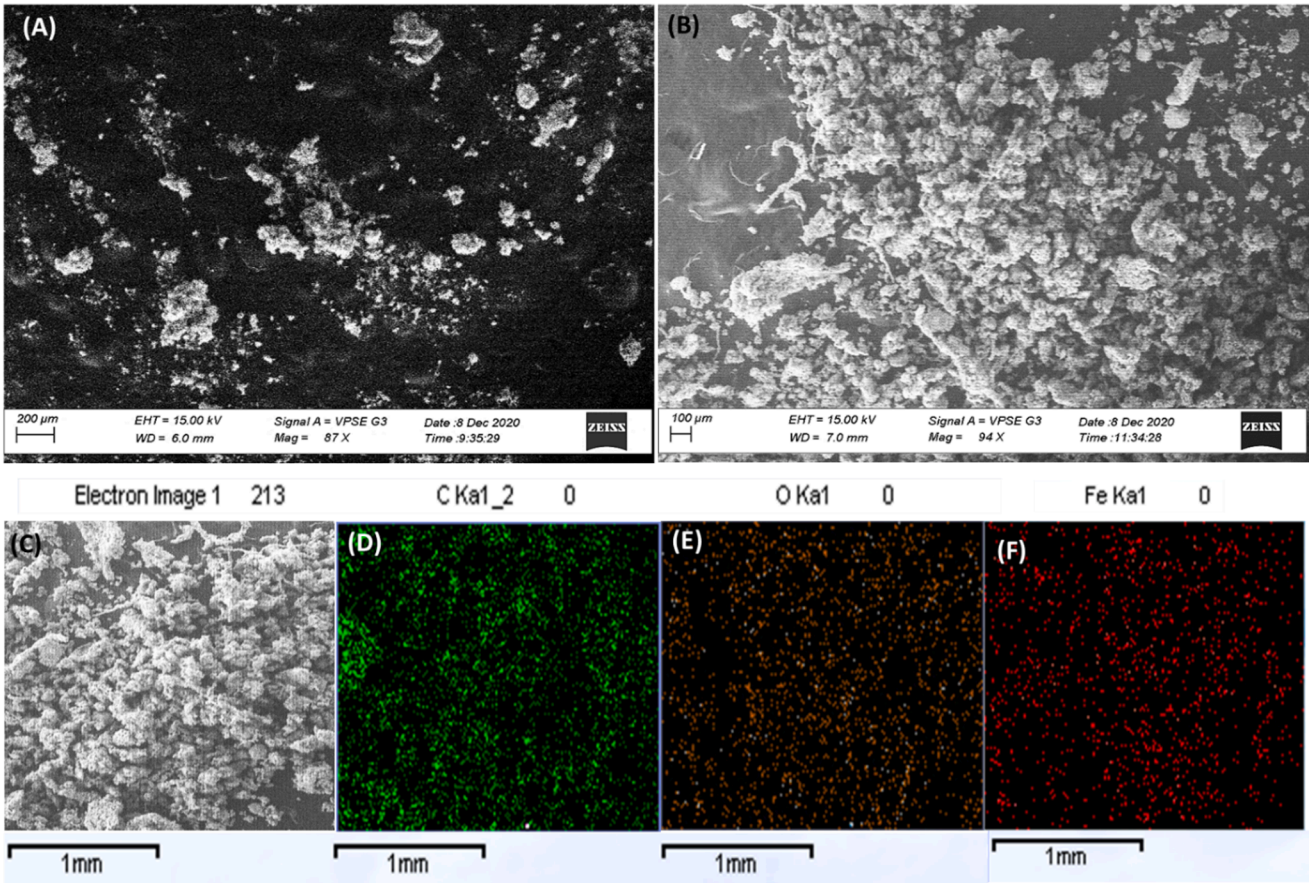

Fig. 3. SEM images showing the morphology of (A) BR and (B) BC-Fe(0) composite material (C)-(F) Elemental mapping images of the respective elements of the BC-Fe(0) composite material.

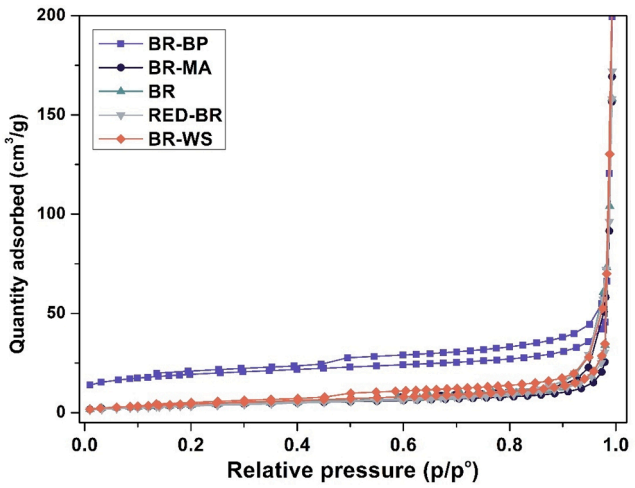

Fig. 4. Adsorption-desorption isotherms (N_2, −196 °C) of BR, RED and BR treated with different biomass. (For interpretation of the references to colour in this figure legend, the reader is referred to the web version of this article.)

display also the predominant presence of macropores. Average pore size results reported in Table S2 can be explained considering the balance between the amount of micro, meso and macropores in the samples. For instance, sample BR BP, corresponding to the lowest average pore size, shows the highest content of mesopores and the lowest of macropores and the presence of micropores.

3.2. Catalytic HTL

Fig. 5A visualizes the distribution of HTL products obtained using biopulp as biomass in non-catalytic and catalytic experiments. The non-catalytic HTL experiment yielded 38.6 wt% of bio-crude oil followed by 34.1 wt% of aqueous phase-soluble organics and 19.9 wt% of gaseous products.

The high lipid content of biopulp probably originating from waste cooking oil, results in higher bio-crude production than many other feedstocks. To leverage the maximum value of biomass, 10 wt% of the synthesized BC-Fe(0) composite material was added to the reaction medium as a catalyst. The yield of bio-crude significantly increased to 44 wt% in presence of Fe(0). As shown in Equation (10), the reaction of water and Fe(0) promotes the in-situ production of H_2 that can ultimately convert unstable intermediates to bio-crude-ranged stable molecules through catalytic transfer hydrogenation reaction (Huang et al., 2016).

$$3Fe(0)\,(catalyst) + 4H_2O \xrightarrow{HTL} Fe_3O_4 + 4H_2 \quad (10)$$

Fig. 5C explicitly illustrates the higher H_2 production in the presence of BC-Fe(0) composite material, which confirms the above explanation. Moreover, the introduced catalyst can facilitate the degradation of biomass constituents' polymeric chain and convert them to bio-crude ranged molecules. However, a meaningful increment in solid residue yield is also observed, which questions the occurrence of the above-mentioned mechanism. By the addition of BC-Fe(0) composite material (10 wt%), the solid product is elevated from 7.5 wt% in the reference experiment to 9.5 wt%, while aqueous phase yield was reduced to 8.4 wt %. It must be noted that the solid yield was calculated on dry ash free

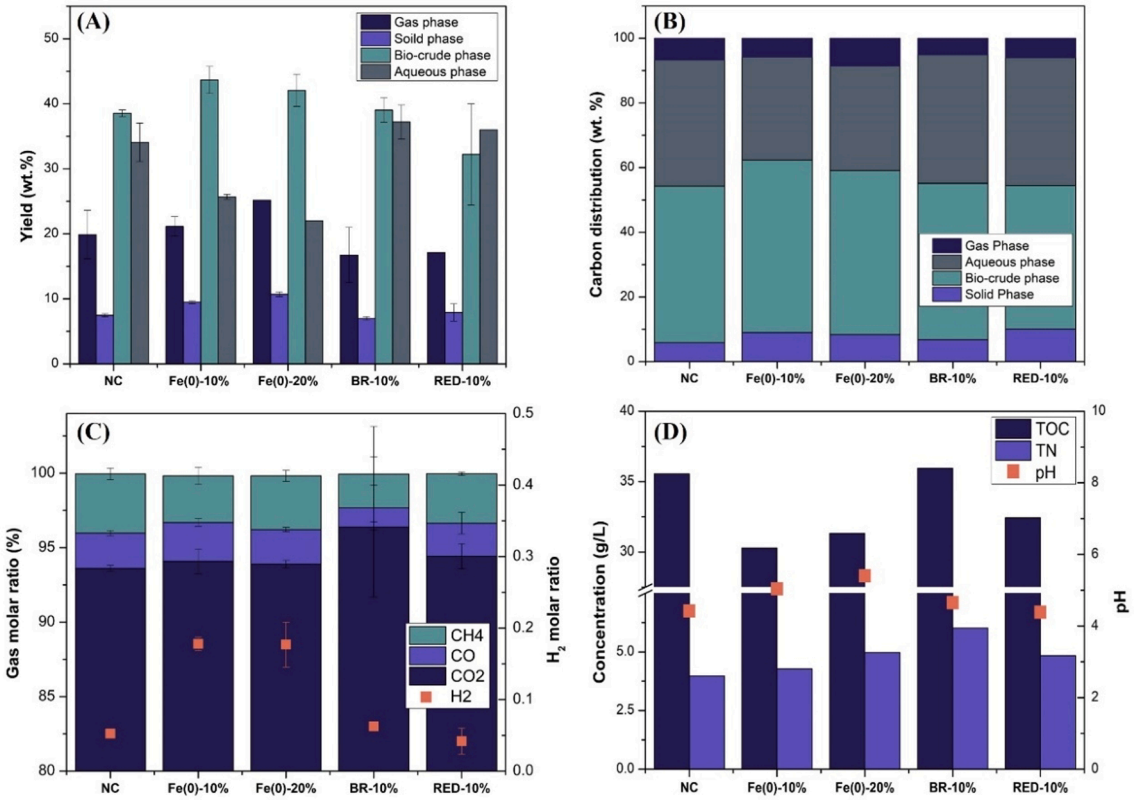

Fig. 5. (A) Product distribution (B) carbon distribution of HTL products with and without catalyst (C) molar distribution of HTL gaseous products and (D) TOC and pH of the aqueous phase samples.

basis by subtracting the total carbon and inorganic content present in the catalyst. The solid residues contain three main constituents such as trapped or strongly adsorbed compounds (volatile matter), residual lignin, and repolymerized phenolics (fixed carbon), and ashes/inorganics (Madsen et al., 2017). As hypothesized, the increment in solid yield is likely due to the adsorption capability of the biochar present in the catalyst. Light organic compounds might be trapped in the biochar, resulting in a lower concentration of organics in the aqueous phase and a higher solid residue (Zhang et al., 2020).

The adsorption of soluble inorganics is another possible pathway that can increase the solid residue yield. However, as shown by Fig. 5B, in the Fe(0)-10 % case, the carbon share in solids is increased by 2.9 wt% than that from the reference test, which confirms the adsorption of the organic molecules. To prove the above-mentioned hypothesis, a duplicated HTL experiment with 6.4 g of HTL aqueous phase (as feedstock) and 0.1 g of BC-Fe(0) material (the same amount of aqueous phase and catalyst as in HTL experiments) was conducted. The results revealed that around 4 wt% of the input carbon was absorbed by the catalyst and the final weight of the input catalyst increased by 20%. Fig. 5D, verifies the effect of the utilized catalyst in decreasing the TOC content and increasing the pH of the HTL aqueous phase. The introduction of the Fe (0)-based composite material decreased the TOC and increased the pH by 5.3 g/L and 1, respectively. TN slightly increased with the presence of Fe(0)-based composite material in the reaction medium and levelled to 4.28 and 4.97 g/L, respectively. Moreover, the high adsorption capacity of BC-Fe(0) composite material was further confirmed by the BET surface area, which was found to be higher than other catalytic materials tested for HTL experiment (Table S2) (Sathishkumar et al., 2012). This might be beneficial in decreasing the dependence on a post-wastewater treatment facility. It is noteworthy that due to the relatively same gas yield and CO_2 content in the reference test and Fe(0)-10 % experiments, the elevation of pH is unlikely to result from the decarboxylation reaction of the light carboxylic acids. Increasing the loading of Fe(0)-20 % slightly decreased the bio-crude yield and favored the production of gaseous molecules. In comparison to the Fe(0)-10 % case, the gaseous products and the share of carbon in the gas phase increased by 4.1 wt% and 2.8 wt%, respectively, while the aqueous phase yield tended to decrease. The reduction of bio-crude yield accompanied with the enhancement of gaseous products yield is likely resulted from the cracking of oil constituents to form gaseous compounds (Zhao et al., 2021). Unanimously, Zhao et al. (2021) reported that along with increasing of Fe dosage to 10 wt% (subcritical HTL of cornstalk), a plateau in bio-crude yield was observed. However, with the further increment of Fe dosage to 25 wt%, a slight reduction in bio-crude yield was observed. Moreover, the summation of the aqueous phase and gaseous products yield enhanced along with the increase of the catalyst loading.

To highlight the specific role of Fe(0), the raw and reduced bauxite residue were separately tested as catalysts in the HTL reaction. Introducing BR to the HTL medium did not change the bio-crude and aqueous phase yields significantly compared to the reference test. Instead, solid, and gaseous products were slightly decreased in the presence of BR. For instance, the gas yield dropped by 3.2 wt% after the addition of raw BR. Cheng et al. (2020) evaluated the impact of some constituent oxides including Fe_2O_3 on the HTL of food waste (Cheng et al., 2020). Despite some variation in the carbon yield of by-products, the bio-crude carbon share was negligibly increased while using ferric oxide (Fe_2O_3) as the main catalyst. In this study, notwithstanding the slight variations in the mass distribution of the products, the carbon share in different phases is on par with what is observed in the reference experiment. The H_2 reduction of raw BR through which the hematite converts to magnetite (Fe_3O_4) was performed to generate the last BC-Fe(0) material. With the introduction of the reduced BR (RED) to the HTL medium, the bio-crude yield conspicuously decreased. However, it should be taken into consideration that the reduction is within the standard deviation range of the reference test. Rahman et al. (2021) performed a series of HTL

experiments using calcinated and reduced BR (at 700 °C) as the prime catalysts (Rahman et al., 2021). It has been notified that under an N_2 atmosphere, both calcinated and reduced catalysts made the bio-crude yield inferior compared to that from the reference test. The asserted statement is in good agreement with the findings of this study.

Thereupon, as suggested by Miyata et al., (2017) the promotion of bio-crude yield with the addition of Fe-based catalysts could be attributed to a) conversion of Fe to Fe_2O_3, which can ultimately enhance the degradation of the biomass polymeric constituents and b) stabilization of the generated intermediates and transferring them to the oil phase (Miyata et al., 2017). Based on the conducted experiments and aforementioned information, this study concludes the second route as the main pathway in bio-crude yield enhancement in the presence of Fe-based catalysts.

3.3. Characterization of HTL products

The results of CHN, yield, HHV, and ER of bio-crude produced with and without using Fe-based catalysts are presented in Table 1. To describe the degree of in-situ hydrogenation and deoxygenation, the H/C and O/C ratios are visualized in Fig. S2 (supporting information).

As compared to the non-catalytic experiment, the Fe(0)-based catalysts slightly increased the carbon and hydrogen contents, therefore H/C ratio of biocrudes is raised using both 10 wt% and 20 wt% of the catalyst. As mentioned before, this might be due to the in-situ hydrogen production of Fe(0)-water reaction, which could be consumed by unstable intermediates and shift the organics to the bio-crude phase over other by-products. Moreover, the generated hydrogen promoted the deoxygenation reactions of oxygenated compounds present in BP through catalytic transfer hydrogenation and resulted in lower oxygen content (and O/C) in the bio-crude derived from the zerovalent iron-assisted HTL experiments. Due to negligible variation in the total gas (Fig. 5A) and CO_2 production (Fig. 5C) in the Fe(0)-10 % in comparison to the reference case, the deoxygenation reaction is partly accomplished through hydrodeoxygenation reaction. Removal of oxygen by hydrodeoxygenation reaction is indeed favourable since it prevents carbon loss in the gas phase unlike conventional deoxygenation pathways (i.e. –CO_2 and –CO). Fig. 5B explicitly reveals the low carbon share (5.8 wt%) in the gas phase while using a lower dosage of the zerovalent iron catalyst. On the other hand, utilization of a higher dosage of the same catalyst accelerated the oxygen removal through the decarboxylation reaction that subsequently increased the CO_2 production and caused higher carbon loss in the gas phase (8.6 wt%). Unlike oxygen content, the nitrogen content and N/C ratio of the bio-crude obtained from the Fe (0)-assisted HTL experiments did not change dramatically. This is likely owing to (a) the high activation energy required for in-situ denitrogenation of bio-crude-ranged molecules and/or (b) polymerization of the N-containing intermediates that can subsequently offset the removed nitrogen (Castello et al., 2019). Collectively, due to the bi-functionality of the Fe(0)-based catalysts in increasing the yield and the quality of bio-crude, ER was significantly enhanced by 14.5 and 11.5 % with the usage of the Fe(0)-10 % and Fe(0)-20 %, respectively.

Raw BR and RED catalysts on the other hand decreased the carbon content of the bio-crude. Unlike the aforementioned catalysts, the utilization of iron oxide (BR and RED) leads to higher oxygen content and O/C ratio than the reference bio-crude. Given the assumption that these catalysts were mainly composed of Fe_2O_3 and Fe_3O_4 respectively, hematite and magnetite revealed no hydrodeoxygenation or decarboxylation/decarbonylation reactions. Hence the HHV in both cases was dropped in comparison to the reference bio-crude. As pointed out previously, these catalysts demonstrated an unsatisfactory performance in bio-crude production and thus, led to lower ER.

The thermal decomposition of solid residue and bio-crudes was analysed via TGA and the results are depicted in Fig. 6A. In the framework of bio-crudes, heating under an N_2 atmosphere caused a weight loss of 82 to 86 %. The negligible weight loss before 150 °C is attributed to the moisture and/or light organics like the residual extraction solvent (DCM) (Kohansal et al., 2019). Relatively small weight loss in this temporal range (50–150 °C) heralds accurate solvent evaporation. The majority (77 to 80 %) of the bio-crude compounds were volatilized in the temperature range of 150–475 °C, which corresponds to the decomposition and evaporation of diesel and its counterpart fractions. According to the DTG graph (Fig. 6B) with the introduction of the BC-Fe (0) (10 wt%) and RED catalysts, the major mass loss peak at around (275 °C) did not significantly change. On the other hand, the higher dosage of BC-Fe(0) catalyst slightly diminished the peak, whereas BR considerably enlarged the peak at around 400 °C. The shift toward higher temperatures is likely due to secondary reactions i.e., repolymerization of oxygen-containing compounds and production of heavier molecules. Another possible reason could be the hydration of the olefins in the acidic condition (pH values in Fig. 5D), which ultimately heightens the boiling of the newly formed molecules more than former precursors.

The result of elemental analysis (Table 1) confirms the occurred phenomenon, where the oxygen content (11.73 wt%) in the bio-crude derived from the BR-assisted experiments was higher than the other bio-crudes. The occurrence of the mentioned reaction will be further discussed by ^{13}C NMR. Furthermore, to have an estimation of the ash content of the solid residue (herein with catalyst) and bio-crudes, the N_2 was switched to O_2 at 775 °C during TGA analysis according to the ASTM E1131-08, which resulted in the oxidation of the residual compounds. As can be seen, all bio-crudes revealed negligible ash content, therefore in the calculations of oxygen content and bio-crude yield (Table 1) the ash content was set aside. Conversely, the solid residues revealed a considerable quantity of ash. The non-catalytic driven solid residue possessed around 38.7 wt% of inorganics, which merely originated from HTL feedstock. However, in the catalytic solid residues the amount of ash substantially increased, due to the share of inorganics originating from the catalyst itself. The solid residue obtained from BR had the highest share of ash (66 wt%) followed by RED, Fe(0)-20 %, and Fe(0)-10 %. Moreover, the higher volatile matter (180–550 °C) and fixed carbon (550–775 °C) found in the non-catalytic case are attributed to the higher share of carbon, than those from the catalytic cases. It can also be seen that the solid residue obtained by Fe(0)-10 % and Fe(0)-20 % had a higher volatile matter and fixed carbon than those from BR and RED, resulting from the synthesis mechanism.

Table 1
Results of elemental analysis, higher heating value, energy recovery, and bio-crude production yield.

Sample	Elemental analysis				O/C	H/C	N/C	HHV_{DAF}	Yield	ER
	C	H	N	O						
Unit	wt.%	wt.%	wt.%	wt.%	–	–	–	MJ/kg	wt.%	%
NC	75.28 ± 0.26	10.36 ± 0.02	4.00 ± 0.08	10.36 ± 0.36	0.11	1.68	0.045	37.81	38.56	65.44
Fe(0)-10 %	75.34 ± 0.70	10.87 ± 0.37	4.02 ± 0.28	9.78 ± 0.04	0.097	1.72	0.046	38.20	43.67	74.85
Fe(0)-20 %	75.53 ± 0.39	10.55 ± 0.15	3.89 ± 0.08	10.04 ± 0.62	0.099	1.70	0.044	38.61	42.07	72.89
BR-10 %	73.91 ± 0.21	10.73 ± 0.08	3.63 ± 0.05	11.73 ± 0.07	0.12	1.73	0.042	37.70	39.03	65.93
RED-10 %	74.68 ± 0.36	10.52 ± 0.07	3.44 ± 0.39	11.37 ± 0.82	0.11	1.68	0.039	37.74	32.22	54.49

DAF = Dry ash free basis.

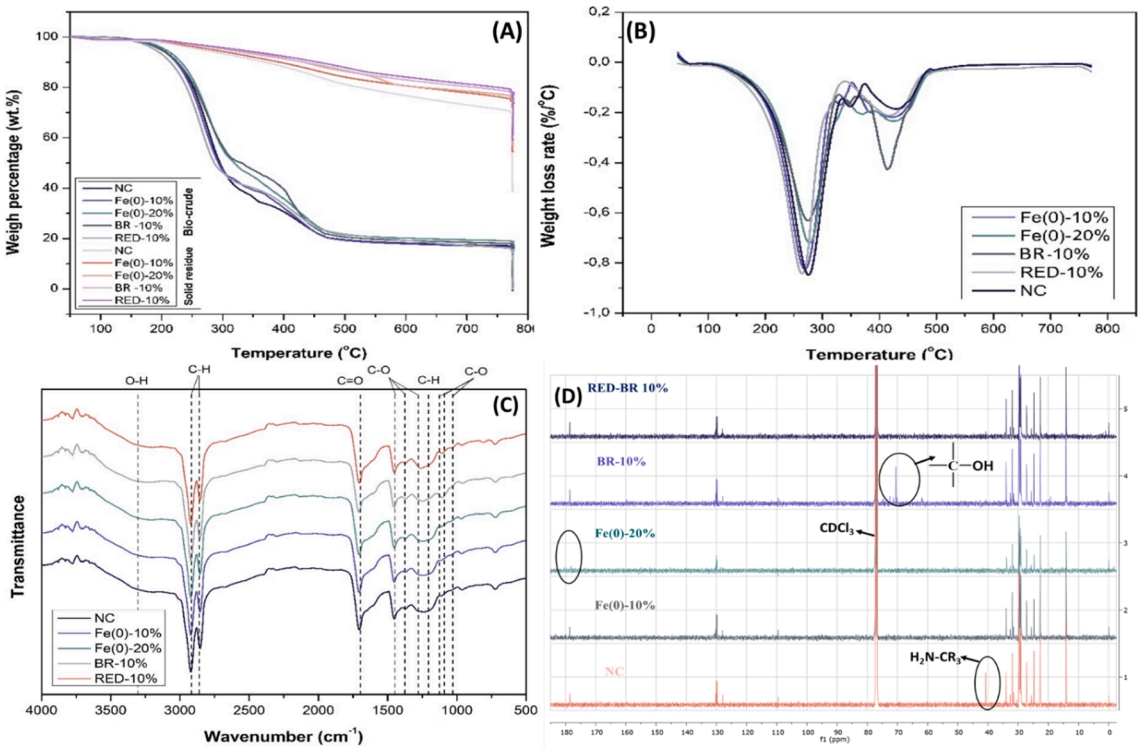

Fig. 6. (A) Thermogravimetric analysis of bio-crude and solid residues (B) differentiated thermogravimetric analysis of bio-crudes (C) FT-IR and (D) ^{13}C NMR spectra of bio-crudes.

As presented in FT-IR (Fig. 6C), similar major functional groups were found in all bio-crudes leading to difficulties in drawing a definite conclusion about the variations caused by different catalysts. The broad peak at around 3300 cm^{-1} is ascribed to the O–H stretching vibration of hydroxyl functional groups in carboxylic acids, alcohols, and phenols. As mentioned before, the higher dosage (20 wt%) of BC-Fe(0) material favored the decarboxylation reaction with the expense of lower hydrodeoxygenation, which causes a slight peak intensity reduction at 3300 cm^{-1}. The asymmetrical and symmetrical stretching vibration of C—H (alkyl groups) appear at 2840 and 3000 cm^{-1}, respectively (Zhao et al., 2021). The strong absorbance peak located at 1700 cm^{-1} indicates the C═O stretching vibration possibly attributed to ketone functionality and/or the carbonyl group of carboxylic acids. The weak shoulder at 1680 cm^{-1} is attributed to the C═C stretching vibration. The absorbance peaks at 1203 cm^{-1}, 1112 cm^{-1}, and 1047 cm^{-1} are related to the C—O stretching vibrations of ethers, esters, and alcohols. The spectrum related to the BR-assisted bio-crude revealed a sharp peak enhancement at 1112 cm^{-1} (related to C—O stretching vibration), suggesting the formation of single bond O-containing functional groups, which was previously indicated by TGA results. Furthermore, the relatively weak absorbance peak at around 1384 cm^{-1} is corresponding to the bending vibration of methylene and/or methyl groups. The C—O stretching vibration of syringyl and guiacyl rings emerged at 1325 and 1270 to 1210 cm^{-1}, respectively (Meier et al., 1986).

To deduce the associated conversion route of biomass and chemical composition of different bio-crudes produced using different Fe-based catalytic materials, ^{13}C NMR spectra of all samples were recorded and the corresponding ^{13}C NMR overlay spectra are shown in Fig. 6D. A quantitative evaluation of the chemical functional groups present in all samples was also carried out through the integration of specific regions according to different chemical shift values of ^{13}C NMR spectra. The observed chemical composition concerning the chemical shift range of

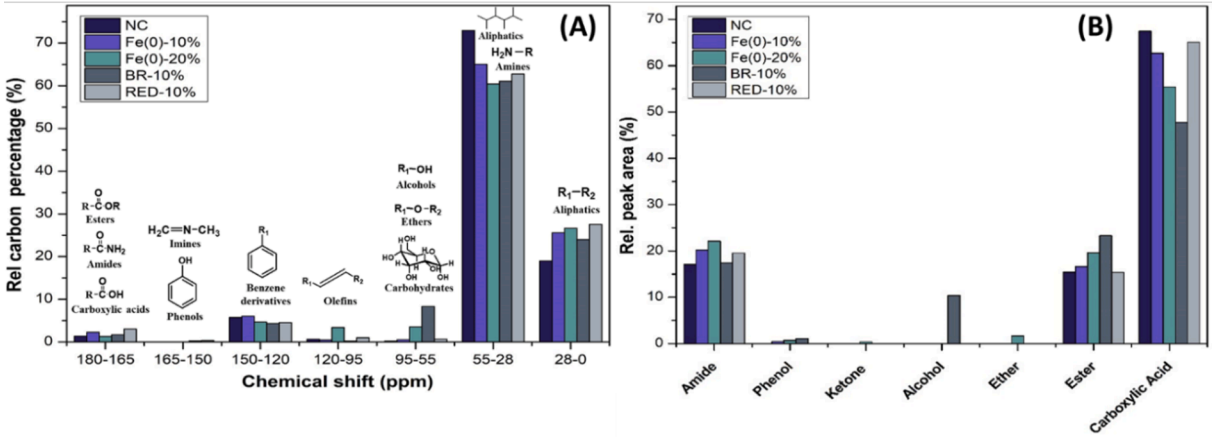

Fig. 7. (A) Quantitative analysis of ^{13}C NMR spectra of produced bio-crudes and (B) categorized organic functional groups in bio-crudes detected by GC–MS.

all samples from ^{13}C NMR analysis is displayed in Fig. 6D.

As shown in Fig. 7A, each spectrum was divided into seven different chemical shift ranges corresponding to different functional groups. The ^{13}C NMR results revealed the presence of carboxylic acids, aromatics, olefins, aliphatic amines, cyclic or branched, and acyclic aliphatics in obtained bio-crudes. The bio-crude produced under non-catalytic conditions showed the presence of carboxylic acids (178.5 ppm), aromatics (128–130.5 ppm), olefins (110 ppm), aliphatic amines (40.7 ppm), and aliphatics (0–28 ppm). These chemical precursors are associated with the lipids, proteins, and lignocellulose components present in the BP feedstock. However, all catalysts involved in the catalytic cleavage of the aliphatic amines or amino acids present in biomass into ammonia, as the peak corresponds to the carbon adjacent to nitrogen (40.7 ppm) disappeared in the bio-crudes obtained using catalysts. Unanimously, Table 1 confirms the removal of amines through the reduction in nitrogen content and N/C ratio. However, unvaried nitrogen contents of bio-crude obtained using Fe(0)-10 % catalyst is likely due to the formation of Maillard products, as the aromatic content of biocrude is slightly increased (Fig. 7A). The high concentration of BC-Fe(0) material induced the hydrodeoxygenation and decarboxylation of fatty acid components of BP as evident from the disappearance of the peak at 178.5 ppm in the NMR spectrum. However, Fe(0)-20 % extensively reduced the relative peak related to carboxylic acid carbons (165–180 ppm) resulting from favoring decarboxylation over hydrodeoxygenation. As mentioned before, the higher share of carbon in gaseous products belonged to the Fe(0)-20 % test confirming the occurrence of the decarboxylation reaction. Furthermore, the increased olefinic contents in the NMR spectrum of bio-crude obtained with Fe(0)-20 % catalyst is likely due to the dehydration of sugar derivatives (e.g. glycerol). However, the NMR spectrum of bio-crude produced using BR showed the presence of alcohols, which was also confirmed by the highest oxygen contents of bio-crude (11.7 wt%) (Table 1 and Fig. 6D). The alcohol functionalities may be formed because of the acidic hydration of olefins, as the BR contains hydroxyl groups (—OH^-) on its surface (Fig. S3). The higher concentration of hydrocarbons (aliphatics) present in the NMR spectra of all bio-crudes in the methylenic region (10–35 ppm) correspond to the resonances of methyl (—CH_3) and methylene (—CH_2-) carbons (saturated and unsaturated) from the fatty acyl chains.

The chemical compounds of bio-crudes derived from catalytic and non-catalytic experiments are quantitatively categorized by GC–MS in Fig. 7B. Note that the analysis only represents the compounds with a boiling point below 320 °C. Based on TGA curves, around 50 to 60 wt% of compounds were identified through GC–MS. All analyzed samples were mainly composed of carboxylic acids, esters, amides, alcohols, ketones, phenols, and ethers. As mentioned before, BR revealed a significant alcohol content that possibly originated from secondary reactions like acidic hydration, while in presence of Fe(0) catalysts such a reaction did not happen. Furthermore, higher ester content is possibly obtained by a secondary esterification reaction of alcohols and carboxylic acids in the acidic HTL medium. Therefore, the carboxylic acid content of bio-crude achieved using BR as the catalyst is relatively decreased. This observation can be confirmed by complying with the higher gas production (Fig. 5A) results and O/C content of the bio-crude (0.12). On the other hand, the carboxylic content of the bio-crude achieved from Fe(0)-10 % catalyst was slightly decreased, which as mentioned before is caused by the hydrodeoxygenation of acids, therefore resulting in lower carbon loss in the gaseous phase. Fe(0)-20 % revealed higher carboxylic acid removal in the lighter fraction of bio-crude due to proceeding the deoxygenation through decarboxylation and hydrodeoxygenation.

Fig. S4 shows the detailed reaction pathways for the formation of various reaction intermediates as components of biocrude oil. Basically, BP contains lignin, hemicellulose, cellulose, protein, and lipid as the main constituents, which undergo hydrolysis to produce derivatives of different functional groups. These derivatives further undergo different chemical reactions and produce monomers and short-chain chemical compounds (Lu et al., 2017). Particularly, short-chain carboxylic acids, alcohols, and ammonia produced from the dehydration, decomposition, and deamination of hemicellulose, cellulose, and proteins are ended up in the aqueous phase. Whereas the furfural derivatives and short-chain ketones produced through the decomposition of hemicellulose and cellulose contributed to the biocrude oil. Maillard reaction between the monosaccharide and amino acids at lower temperatures through cyclization generated N-heterocyclic compounds in the biocrude phase. However, the amides can be generated under hydrothermal conditions through the condensation reaction between long-chain carboxylic acids and amines (Fu et al., 2020).

4. Conclusion

In this study, BC-Fe(0) composite material was successfully synthesized from BR through a one-step green recycling route using biopulp as a reducing agent. Different characterization techniques were used to interpret BC-Fe(0) material, which confirmed the presence of zerovalent iron. Despite using low catalyst loading (10 wt%) of BC-Fe(0) material (containing 2.5 wt% Fe) for HTL of BP, substantial hydrodeoxygenation of organic compounds was achieved, which reflects the high catalytic activity of synthesized material and improved quality of bio-crude. Specifically, the resulting bio-crude exhibited a higher H/C ratio (1.73) and lower oxygen contents (9.78 wt%) in comparison to the bio-crude obtained without using any catalyst under similar conditions. Furthermore, the bio-crude yield (44 wt%) was also considerably higher than non-catalytic (38.6 wt%) as well as other iron-based oxide catalysts like raw BR (40 wt%) and reduced BR (RED) (32 wt%) tested in this study. These results show the effectiveness of the current method for the green reduction of bauxite residue and the high catalytic efficiency of synthesized material for the valorization of MSW. This method can be an effective alternative to the existing chemical-based industrial waste recycling and catalysts synthesis processes.

Declaration of Competing Interest

The authors declare that they have no known competing financial interests or personal relationships that could have appeared to influence the work reported in this paper.

Data availability

No data was used for the research described in the article.

Acknowledgement

Authors are thankful to the Mytilineos Holdings S.A, Greece for providing the bauxite residue. This research acknowledges support from “Urban Waste Hydrofaction” project, funded by the Energy Technology Development and Demonstration Program (EUDP).

Appendix A. Supplementary material

Supplementary data to this article can be found online at https://doi.org/10.1016/j.wasman.2023.08.024.

References

Afonso, M.D.S., Morando, P.J., Blesa, M.A., Banwart, S., Stumm, W., 1990. The reductive dissolution of iron oxides by ascorbate: The role of carboxylate anions in accelerating reductive dissolution. J. Colloid Interface Sci. 138, 74–82. https://doi.org/10.1016/0021-9797(90)90181-M.

Agblevor, F.A., Wang, H., Beis, S., Christian, K., Slade, A., Hietsoi, O., Santosa, D.M., 2020. Reformulated Red Mud: a Robust Catalyst for In Situ Catalytic Pyrolysis of Biomass. Energy Fuels 34, 3272–3283. https://doi.org/10.1021/acs.energyfuels.9b04015.

Ansari, M.A., Asiri, S.M.M., Alzohairy, M.A., Alomary, M.N., Almatroudi, A., Khan, F.A., 2021. Biofabricated Fatty Acids-Capped Silver Nanoparticles as Potential Antibacterial, Antifungal, Antibiofilm and Anticancer Agents. *Pharmaceuticals* 14, 139. https://doi.org/10.3390/ph14020139.

Barrett, E.P., Joyner, L.G., Halenda, P.P., 1951. The determination of pore volume and area distributions in porous substances. I. Computations from nitrogen isotherms. J. Am. Chem. Soc. 73, 373–380. https://doi.org/10.1021/ja01145a126.

Brunauer, S., Emmett, P.H., Teller, E., 1938. Adsorption of gases in multimolecular layers. J. Am. Chem. Soc. 60, 309–319. https://doi.org/10.1021/ja01269a023.

Cardenia, C., Balomenos, E., Panias, D., 2019. Iron Recovery from Bauxite Residue Through Reductive Roasting and Wet Magnetic Separation. J. Sustain. Metall. 2019 (5), 9–19. https://doi.org/10.1007/s40831-018-0181-5.

Castello, D., Haider, M.S., Rosendahl, L.A., 2019. Catalytic upgrading of hydrothermal liquefaction biocrudes: Different challenges for different feedstocks. Renew. Energy 141, 420–430. https://doi.org/10.1016/j.renene.2019.04.003.

Chen, D.-M.-C., Bodirsky, B.L., Krueger, T., Mishra, A., Popp, A., 2020. The world's growing municipal solid waste: trends and impacts. Environ. Res. Lett. 15, 074021 https://doi.org/10.6084/m9.figshare.12102510.

Chen, W.-T., Zhang, Y., Lee, T.H., Wu, Z., Si, B., Lee, C.-F.-F., Lin, A., Sharma, B.K., 2018. Renewable diesel blendstocks produced by hydrothermal liquefaction of wet biowaste. Nature Sustain. 1, 702–710. https://doi.org/10.1038/s41893-018-0172-3.

Chen, H., Zheng, Z., Chen, Z., Bi, X.T., 2017. Reduction of hematite (Fe_2O_3) to metallic iron (Fe) by CO in a micro fluidized bed reaction analyzer: A multistep kinetics study. Powder Technol. 316, 410–420. https://doi.org/10.1016/j.powtec.2017.02.067.

Cheng, F., Tompsett, G.A., Murphy, C.M., Maag, A.R., Carabillo, N., Bailey, M., Hemingway, J.J., Romo, C.I., Paulsen, A.D., Yelvington, P.E., Timko, M.T., 2020. Synergistic Effects of Inexpensive Mixed Metal Oxides for Catalytic Hydrothermal Liquefaction of Food Wastes. ACS Sustain. Chem. Eng. 8 (17), 6877–6886. https://doi.org/10.1021/acssuschemeng.0c02059.

Conti, F., Toor, S.S., Pedersen, T.H., Seehar, T.H., Nielsen, A.H., Rosendahl, L.A., 2020. Valorization of animal and human wastes through hydrothermal liquefaction for biocrude production and simultaneous recovery of nutrients. Energy Convers. Manage. 216, 112925 https://doi.org/10.1016/j.enconman.2020.112925.

European Commission, Study on the EU's list of Critical Raw Materials (2020), Factsheets on Critical Raw Materials.

Fu, X., Liao, Y., Glein, C.R., Jamison, M., Hayes, K., Zaporski, J., Yang, Z., 2020. Direct Synthesis of Amides from Amines and Carboxylic Acids under Hydrothermal Conditions. ACS Earth Space Chem. 4 (5), 722–729. https://doi.org/10.1021/acsearthspacechem.0c00009.

Gasparatos, A., Stromberg, P., Takeuchi, K., 2013. Sustainability impacts of first-generation biofuels. Animal Frontiers 3, 12–26. https://doi.org/10.2527/af.2013-0011.

Guo, Z., Bai, G., Huang, B., Cai, N., Guo, P., Chen, L., 2021. Preparation, and application of a novel biochar-supported red mud catalyst: Active sites and catalytic mechanism. J. Hazard. Mater. 408, 124802 https://doi.org/10.1016/j.jhazmat.2020.124802.

Huang, Y.-X., Guo, J., Zhang, C., Hu, Z., 2016. Hydrogen production from the dissolution of nano zero valent iron and its effect on anaerobic digestion. Water Res. 88, 475–480. https://doi.org/10.1016/j.watres.2015.10.028.

Klačanová, K., Fodran, P., Šimon, P., Rapta, P., Boča, R., Jorík, V., Miglierini, M., Kolek, E., Čaplovič, L.'., 2013. Formation of Fe(0)-Nanoparticles via Reduction of Fe (II) Compounds by Amino Acids and Their Subsequent Oxidation to Iron Oxides. *J. Chem.* 1–10. https://doi.org/10.1155/2013/961629.

Klauber, C., Gräfe, M., Power, G., 2009. Review of Bauxite Residue "Re-use'' Options. CSIRO Document DMR-3609.

Kohansal, K., Tavasoli, A., Bozorg, A., 2019. Using a hybrid-like supported catalyst to improve green fuel production through hydrothermal liquefaction of Scenedesmus obliquus microalgae. Bioresour Technol. 277, 136–147. https://doi.org/10.1016/j.biortech.2018.12.081.

Kohansal, K., Sharma, K., Toor, S.S., Sanchez, E.L., Zimmermann, J., Aistrup Rosendahl, L., Pedersen, T.H., 2021b. Bio-Crude Production Improvement during Hydrothermal Liquefaction of Biopulp by Simultaneous Application of Alkali Catalysts and Aqueous Phase Recirculation. Energies 14 (15), 4492. https://doi.org/10.3390/en14154492.

Kohansal, K.K., Toor, S., Sharma, K., Chand, R., Rosendahl, L., Pedersen, T.H., 2021a. Hydrothermal liquefaction of pre-treated municipal solid waste (biopulp) with recirculation of concentrated aqueous phase. Biomass Bioenergy 148, 106032. https://doi.org/10.1016/j.biombioe.2021.106032.

Limo, M.J., Sola-Rabada, A., Boix, E., Thota, V., Westcott, Z.C., Puddu, V., Perry, C.C., 2018. Interactions between Metal Oxides and Biomolecules: from Fundamental Understanding to Applications. Chem. Rev. 118, 11118–11193. https://doi.org/10.1021/acs.chemrev.7b00660.

Lu, J., Zhang, J., Zhu, Z., Zhang, Y., Zhao, Y., Li, R., Watson, J., Li, B., Liu, Z., 2017. Simultaneous production of biocrude oil and recovery of nutrients and metals from human feces via hydrothermal liquefaction. Energy Convers. Manage. 134, 340–346. https://doi.org/10.1016/j.enconman.2016.12.052.

Madsen, R.B., Jensen, M.M., Glasius, M., 2017. Qualitative characterization of solid residue from hydrothermal liquefaction of biomass using thermochemolysis and stepwise pyrolysis-gas chromatography-mass spectrometry. Sustain. Energy Fuels 1, 2110–2119. https://doi.org/10.1039/C7SE00357A.

Masud, A., Soria, N.G.C., Aga, D.S., Aich, N., 2020. Adsorption and advanced oxidation of diverse pharmaceuticals and personal care products (PPCPs) from water using highly efficient rGO–nZVI nanohybrids. Environ. Sci.: Water Res. Technol. 6, 2223–2238. https://doi.org/10.1039/d0ew00140f.

Meier, D., Larimer, D.R., Faixa, O., 1986. Direct liquefaction of different lignocellulosics and their constituents: 2. Molecular weight determination, gas chromatography, i.r. spectroscopy. Fuel 65, 916–921. https://doi.org/10.1016/0016-2361(86)90198-5.

Miyata, Y., Sagata, K., Hirose, M., Yamazaki, Y., Nishimura, A., Okuda, N., Arita, Y., Hirano, Y., Kita, Y., 2017. Fe-Assisted Hydrothermal Liquefaction of Lignocellulosic Biomass for Producing High-Grade Bio-Oil. ACS Sustainable Chem. Eng. 5 (4), 3562–3569. https://doi.org/10.1021/acssuschemeng.7b00381.

Mombelli, D., Mapelli, C., Barella, S., Gruttadauria, A., Spada, E., 2019. Jarosite wastes reduction through blast furnace sludges for cast iron production. J. Environ. Chem. Eng. 7 (2), 102966. https://doi.org/10.1016/j.jece.2019.102966.

Ouyang, D., Yan, J., Qian, L., Chen, Y., Han, L., Su, A., Zhang, W., Ni, H., Chen, M., 2017. Degradation of 1,4-dioxane by biochar supported nano magnetite particles activating persulfate. Chemosphere 184, 609–617. https://doi.org/10.1016/j.chemosphere.2017.05.156.

Posmanik, R., Martinez, C.M., Cantero-Tubilla, B., Cantero, D.A., Sills, D.L., Cocero, M.J., Tester, J.W., 2018. Acid and Alkali Catalyzed Hydrothermal Liquefaction of Dairy Manure Digestate and Food Waste. ACS Sustain. Chem. Eng. 6 (2), 2724–2732. https://doi.org/10.1021/acssuschemeng.7b04359.

Rahman, T., Jahromi, H., Roy, P., Adhikari, S., Hassani, E., Oh, T.-S., 2021. Hydrothermal liquefaction of municipal sewage sludge: Effect of red mud catalyst in ethylene and inert ambiences. Energy Convers. Manage. 245, 114615 https://doi.org/10.1016/j.enconman.2021.114615.

Ross, A.B., Biller, P., Kubacki, M.L., Li, H., Lea-Langton, A., Jones, J.M., 2010. Hydrothermal processing of microalgae using alkali and organic acids. Fuel 89, 2234–2243. https://doi.org/10.1016/j.fuel.2010.01.025.

Saffari, M., 2018. Response surface methodological approach for optimizing the removal of cadmium from aqueous solutions using pistachio residues biochar supported/non-supported by nanoscale zero-valent iron. Main Group Metal Chem. 41, 167–181. https://doi.org/10.1515/mgmc-2018-0011.

Sathishkumar, P., Arulkumar, M., Palvannan, T., 2012. Utilization of agro-industrial waste Jatropha curcas pods as an activated carbon for the adsorption of reactive dye Remazol Brilliant Blue R (RBBR). J. Clean. Prod. 22, 67–75. https://doi.org/10.1016/j.jclepro.2011.09.017.

Scarsella, M., Caprariis, B., Damizia, M., De, P., 2020. Filippis, Heterogeneous catalysts for hydrothermal liquefaction of lignocellulosic biomass: A review. Biomass Bioenergy 140, 105662. https://doi.org/10.1016/j.biombioe.2020.105662.

Seehar, T.H., Toor, S.S., Shah, A.A., Pedersen, T.H., Rosendahl, L.A., 2020. Biocrude Production from Wheat Straw at Sub and Supercritical Hydrothermal Liquefaction. Energies 13, 3114. https://doi.org/10.3390/en13123114.

Sharma, K.D., Jain, S., 2020. Municipal solid waste generation, composition, and management: the global scenario. Soc. Responsib. J. 16, 917–948. https://doi.org/10.1108/SRJ-06-2019-0210.

Sintamarean, I.M., Pedersen, T.H., Zhao, X., Kruse, A., Rosendahl, L.A., 2017. Application of Algae as Cosubstrate to Enhance the Processability of Willow Wood for Continuous Hydrothermal Liquefaction. Ind. Eng. Chem. Res. 56, 4562–4571. https://doi.org/10.1021/acs.iecr.7b00327.

Taghipour, A., Hornung, U., Ramirez, J.A., Brown, R.J., Rainey, T.J., 2021. Aqueous phase recycling in catalytic hydrothermal liquefaction for algal biomass and the effect on elemental accumulation and energy efficiency. J. Clean. Prod. 289, 125582 https://doi.org/10.1016/j.jclepro.2020.125582.

Ujaczki, É., Feigl, V., Molnár, M., Cusack, P., Curtin, T., Courtney, R., O'Donoghue, L., Davris, P., Hugi, C., Evangelou, M.W., Balomenos, E., Lenz, M., 2018. Re-using bauxite residues: benefits beyond (critical raw) material recovery. J. Chem. Technol. Biotechnol. 93 (9), 2498–2510. https://doi.org/10.1002/jctb.5687.

Wang, H., Cai, J., Liao, Z., Jawad, A., Ifthikar, J., Chen, Z., Chen, Z., 2020b. Black liquor as biomass feedstock to prepare zero-valent iron embedded biochar with red mud for Cr(VI) removal: Mechanisms insights and engineering practicality. Bioresource Technol. 311, 123553 https://doi.org/10.1016/j.biortech.2020.123553.

Wang, X., Li, Z., Bai, X., Zhou, X., Cheng, S., Gao, R., Sun, J., 2018. Study on improving anaerobic co-digestion of cow manure and corn straw by fruit and vegetable waste: methane production and microbial community in CSTR process. Bioresource Technol. 249, 290–297. https://doi.org/10.1016/j.biortech.2017.10.038.

Wang, F., Liu, J., 2014. Liposome Supported Metal Oxide Nanoparticles: Interaction Mechanism, Light Controlled Content Release, and Intracellular Delivery. Small 10, 3927–3931. https://doi.org/10.1002/smll.201400850.

Wang, C., Zhang, X., Sun, R., Cao, Y., 2020a. Neutralization of red mud using bio-acid generated by hydrothermal carbonization of waste biomass for potential soil application. J. Clean. Prod. 271, 1225252. https://doi.org/10.1016/j.jclepro.2020.122525.

Wang, C., Wang, H., Yan, Q., Chen, C., Bao, X., Pan, M., Qian, Y., 2023. Enhanced nitrogen removal from low C/N municipal wastewater employing algal biochar supported nano zero-valent iron (ABC-nZVI) using A/A/O-MBR: Duration and rehabilitation. Sci. Total Environ. 860, 160396 https://doi.org/10.1016/j.scitotenv.2022.160396.

Wang, J., Zhang, W., Kang, X., Zhang, C., 2019. Rapid and efficient recovery of silver with nanoscale zerovalent iron supported on high performance activated carbon derived from straw biomass. Environ. Pollut. 255, 113043 https://doi.org/10.1016/j.envpol.2019.113043.

Yoon, K., Cho, D.-W., Tsang, Y.F., Tsang, D.C.W., Kwon, E.E., Song, H., 2019. Synthesis of functionalised biochar using red mud, lignin, and carbon dioxide as raw materials. Chem. Eng. J. 361, 1597–1604. https://doi.org/10.1016/j.cej.2018.11.012.

Zhang, Y., Jiao, X., Liu, N., Lv, J., Yang, Y., 2020b. Enhanced removal of aqueous Cr(VI) by a green synthesized nanoscale zero-valent iron supported on oak wood biochar. Chemosphere 245, 125542. https://doi.org/10.1016/j.chemosphere.2019.125542.

Zhang, K., Zhong, S., Zhang, H., 2020a. Predicting Aqueous Adsorption of Organic Compounds onto Biochars, Carbon Nanotubes, Granular Activated Carbons, and Resins with Machine Learning. Environ. Sci. Technol. 54, 7008–7018. https://doi.org/10.1021/acs.est.0c02526.

Zhao, B., Hu, Y., Qi, L., Gao, J., Zhao, G., Ray, M.B., Xu, C.C., 2021. Promotion effects of metallic iron on hydrothermal liquefaction of cornstalk in ethanol-water mixed solvents for the production of biocrude oil. Fuel 285, 119150. https://doi.org/10.1016/j.fuel.2020.119150.

Further reading

International Energy Agency, 2015. Energy Technology Perspectives 2015. IEA Publications, Paris, France.